Chemical Science

ROYAL SOCIETY OF CHEMISTRY

EDGE ARTICLE

View Article Online
View Journal

Cite this: DOI: 10.1039/d6sc00974c

All publication charges for this article have been paid for by the Royal Society of Chemistry

Metal cations promote coupled ion–electron transfer during deposition and corrosion

E. I. Stern, K. A. Thurman, F. Brito dos Santos and P. A. Kempler *

During electrodeposition and corrosion reactions, dissolved metal ions transfer across the electrochemical double layer, undergoing changes in their solvation environment and oxidation state. The solvent reorganization during charge transfer is expected to increase with the charge density of the dissolved species, but the mechanistic pathway of cation (de)solvation remains poorly understood. Here, we have quantified the kinetics of underpotential deposition for two ions associated with rapid metal deposition kinetics: Cu^{2+} and Ag^{+}, at site-defined Au(111) surfaces for deposition and corrosion. Both metal adsorbates exhibited reversible adsorption kinetics at low coverage and slow scan rates, along with a symmetric transfer coefficient, $\alpha \sim 1/2$, consistent with a single electron/ion transfer during the rate determining step. The standard rate constant for Ag^{+} transfer was within an order of magnitude of reported adiabatic electron transfer rate constants, and the kinetics of Cu^{2+} transfer were consistent with the rate determining step involving metal adsorption. The self-exchange rate for both Ag^{+} and Cu^{2+} transfer exhibited a reaction order of $\sim 2\alpha$ with respect to cation concentration, indicating that metal cations promote their own ion transfer step and a self-consistent mechanism involving solvent exchange prior to ion transfer is proposed. Insights from this kinetic model could support improved additives for metal deposition in semiconductors, redox-flow battery electrolytes, and electrorefining processes for energy-critical metals.

Received 4th February 2026
Accepted 8th June 2026

DOI: 10.1039/d6sc00974c

rsc.li/chemical-science

Introduction

Electrochemical deposition and corrosion of transition metals are a class of reactions fundamental for batteries, industrial refining of metals, and advanced manufacturing of semiconductor devices. The electrochemical corrosion and deposition of Cu^{2+} is used to refine nearly all Cu metal used in wiring, electronics, and plumbing; advanced embodiments of Cu and Ag deposition are used to form interconnects within nano- to micro-scale vias in most semiconductor devices.[1–3] Nevertheless, the elementary steps associated with aqueous deposition, particularly of multivalent species, remain poorly understood such that strategies to control deposition and corrosion are identified empirically.[4] The microscopic steps associated with transferring a solvated ion across the electrified solid–liquid interface are generally made complicated by ill-defined electric fields, large solvation energies, and a poorly defined population of adsorbates and adsorption sites—collectively, these steps are referred to as interfacial ion transfer, IIT.[5–7] Resolving microscopic steps associated with metal IIT can clarify our understanding of the dynamic structure of electrified interfaces and provide a unifying theory for ion transfer reactions to connect with established theories of electron transfer.[8,9]

The adsorption of a metal cation is an IIT reaction required for electrochemical deposition and should involve (in no particular order) electron transfer(s) to the cation, adsorption to a surface site, loss of the solvation shell, and reorganization of the local double layer structure. Conway claimed that the reduction of Cu^{2+} to Cu^{+} is the rate determining step (RDS) for Cu deposition whereas Ag^{+} IIT becomes the rate determining step for Ag deposition at high overpotentials.[10] The standard rate constants for Co^{2+}, Ni^{2+}, and Fe^{2+} deposition are 10^{3} to 10^{5} times less than those for Ag^{+} and Cu^{2+}, which may be related to the fact that the former metals lack a stable +1 oxidation state.[10] Gileadi noted the curiosities associated with high exchange current densities for metal deposition relative to the comparable rates of outer-sphere electron transfer and proposed a mechanism in which the free energy of the system is lowered through a gradual delocalized electron transfer from the metal to the solvated ion which lowers the energy for the stepwise removal of water molecules.[11] More recent simulations and experiments have suggested that aqueous Ag^{+} may approach within a few angstroms of the surface before undergoing a rapid transfer enabled by favorable interactions between the Ag 5s orbital and a delocalized sp band from the metal.[12,13] These findings provide insights into rapid kinetics for monovalent metal deposition but fail to resolve the more complex picture required for understanding the deposition and corrosion of multivalent metal ions.[14–18]

Department of Chemistry and Biochemistry, The Oregon Center for Electrochemistry, University of Oregon, Eugene, OR, USA. E-mail: pkempler@uoregon.edu

Underpotential deposition (UPD) on site-defined Au surfaces is a well-suited system for addressing the complexities of interfacial ion transfer. UPD is a phenomenon where ions are adsorbed onto the surface at potentials more favorable compared to the standard reduction potential where the deposition would be expected. This phenomenon is caused by more favorable surface–adsorbate interactions compared to the adsorbate adsorbing onto itself. UPD is thus an inherently self-limiting process, and the surface coverage is a state function that can be easily controlled by the applied electrochemical potential. UPD on a wide variety of single crystal surfaces has well characterized surface phases and phase transitions.[19–21] Cu and Ag UPD at Au(111) is a suitable model system to compare the mechanism for IIT for monovalent and divalent metal cations, as both metals have similar lattice constants and exhibit kinetic regions of quasireversible adsorption/desorption. Whereas Cu^{2+} can be repeatedly adsorbed/desorbed from the Au surface, Ag participates in exchange with surface Au atoms which has previously hindered the characterization of Ag^{+} adsorption.[22,23]

Here, we conduct site-defined measurements of transition metal IIT kinetics for Ag^{+} and Cu^{2+} at Au(111) in two non-coordinating electrolytes to develop a microscopic framework for metal deposition and corrosion. The use of an inert and well-defined Au(111) substrate for adsorption allowed kinetics to be quantified with a known number of active sites and a known coverage of adsorbed intermediates, neither of which is possible at a growing/corroding metal surface. Divalent Cu^{2+} adsorption is shown to be controlled by a single charge transfer step with a symmetric transfer coefficient and an adsorbed product. The reaction order of metal ion transfer was quantified with respect to the concentration of dissolved metals and the coverage of intermediates, indicating the presence of a multi-step adsorption mechanism present even for elementary univalent ion transfer.

Experimental methods

Chemicals

Deionized water with a resistivity of 18.2 MΩ cm, DI H_2O, was obtained from a laboratory water purification system (Thermo Scientific Barnstead Nanopure). Perchloric acid ($HClO_4$, 10.25 M, TraceMetal Grade) and sulfuric acid (H_2SO_4 96% aq., TraceMetal Grade) were obtained from Fisher Chemical, whereas silver perchlorate monohydrate (99.999% metals basis) and copper(II) oxide (99.99% trace metals basis) were obtained from Sigma-Aldrich. Silver perchlorate monohydrate and copper(II) oxide were used as sources of Ag^{+} and Cu^{2+}, respectively, for all experiments.

Electrodes

Au(111) surfaces were prepared from thermally evaporated Au (4N) on titanium-coated glass slides (GOLD SEAL®, Electron Microscopy Sciences). Slides were cleaned in an oxygen plasma for 15 min before being transferred to a thin-film deposition system (Angstrom Engineering). A 17 nm adhesion layer of Ti was deposited *via* electron beam evaporation followed by 200 nm of thermally evaporated Au. The as-deposited Au electrodes were annealed under a butane flame and cooled in an Ar(g) stream before being transferred to the cell environment. X-ray diffraction of these surfaces indicated that the surface was primarily oriented to expose the Au(111) surface after annealing (Fig. S1). A flame-cleaned Pt wire (99.997% metals basis, Thermo-Scientific) served as the counter electrode. A high purity Ag wire (99.999%, Thermo-Scientific) or Cu wire (99.999%, Alfa Aesar) served as quasi-reference electrodes and were protected behind a fritted glass pipette filled with an electrolyte identical to that in the cell to avoid contamination. Quasi reference electrodes were checked against a mercury sulfate reference electrode in saturated potassium sulfate (MSE) after voltammetry experiments.

Electrochemistry

Glassware was cleaned in H_2SO_4 with a persulfate-based oxidizing agent (Alnochromix) for >24 h to remove trace contaminants and then boiled three times in DI H_2O. Solutions were purged under ultrahigh purity Ar (99.999%) for at least 15 minutes and kept blanketed with a gentle flow of Ar during experiments. Cu-containing solutions were prepared by dissolving CuO in $HClO_4$ and all Ag-containing solutions were prepared by dissolving $AgClO_4 \cdot H_2O$ in $HClO_4$. All electrochemical data were collected on a Bio-Logic SP-300 potentiostat. Reported electrochemical potentials, E, are referenced to a mercury sulfate electrode (MSE) or the reversible potential for metal deposition at Cu or Ag (E_{rev}). E_{rev} for Cu was ∼−410 mV *vs.* MSE for 1 mM CuO in 100 mM $HClO_4$ and E_{rev} for Ag was ∼−40 mV *vs.* MSE for 1 mM $AgClO_4$ in 99 mM $HClO_4$. Stability of the Au(111) interface was checked by sweeping the potential at a scan rate (ν) of 25 mV s^{-1} until a steady electrochemical response was reached (3–10 cycles). For measurements on Cu adsorption kinetics, the potential was cycled repeatedly from 0.000–0.600 V *vs.* E_{rev} at various ν and the second cycle was used for analysis. For Ag UPD, the surface quality was confirmed using voltammetry at 25 mV s^{-1} and then the potential was stabilized at 0.300 V *vs.* E_{rev} for 10 s before a series of linear sweeps were collected from 0.300 to 0.585 V *vs.* E_{rev} at various ν. For both Cu and Ag, ν was varied from 25 mV s^{-1} to 50 V s^{-1}, with high concentrations of adsorbates or the supporting electrolyte requiring faster ν to observe the impact of kinetics.

Results

Cyclic voltammetry of Cu^{2+} at Au(111)-textured electrodes in $HClO_4$(aq.) yielded a broad adsorption wave from −0.40 to −0.15 V *vs.* MSE with a sharp desorption wave from −0.20 to −0.05 V *vs.* MSE, characteristic of UPD of Cu on Au(111) in $HClO_4$(aq.) (Fig. 1a).[24,25] The current response from $E = -0.15$ to 0.00 V was equal and opposite for the scans in the negative and positive directions, consistent with a reversible adsorption process.

Cyclic voltammetry of Ag^{+} at Au(111)-textured electrodes in $HClO_4$(aq.) yielded a reversible adsorption peak between $E =$

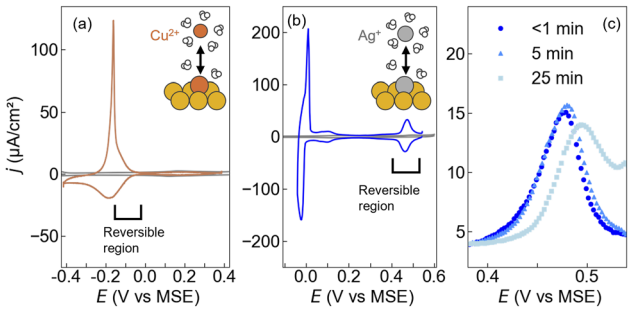

Fig. 1 (a) Cyclic voltammetry of Cu UPD on Au(111) in 0.001 M $Cu(ClO_4)_2$ and 0.098 M $HClO_4$ (0.100 M ClO_4^-). (b) Ag UPD on Au(111) in 0.001 M $AgClO_4$ and 0.099 M $HClO_4$ (0.100 M ClO_4^-). The gray traces in (a) and (b) represent the CV of Au(111) in 0.100 M $HClO_4$. (c) Cyclic voltammetry of Ag UPD on Au(111) in a solution of 0.001 M Ag ClO_4 and 0.099 M $HClO_4$ (0.100 M ClO_4^-) as a function of time spent in solution. All scans were recorded at 25 mV s^{-1} and initially swept in the negative direction.

0.45 and 0.55 V *vs.* MSE, a broad, capacitive region from $E = 0.15$ to 0.50 V, and a sharp irreversible adsorption peak from $E = -0.05$ to 0.05 V; all cathodic charges were balanced by commensurate desorption peaks and were qualitatively consistent with Ag UPD at Au(111) single crystals in $HClO_4$(aq.) (Fig. 1b).[26,27] The total integrated charge from $E = -0.050$ to 0.550 V was 276 μC cm^{-2}, which is consistent with the reported value for Ag^+ adsorption at Au(111) crystals from $HClO_4$ electrolytes and slightly greater than the theoretical value of 222 μC cm^{-2} for a close packed monolayer of Ag. We focused on potential regions yielding reversible and low coverage of adsorbates such that charge passed could be assigned to isolated adsorbates on a site-defined metal surface. The measured current density was normalized to scan rate, j/ν, and all potentials were measured against the equilibrium potential for bulk deposition/corrosion in the working electrolyte.

The stability of Au(111) surfaces in solutions containing Ag^+ was investigated using voltammetry and X-ray photoelectron spectroscopy (XPS). Following the scans for Ag UPD a positive potential shift for the charge in the reversible E region of <5 mV was observed and XPS analysis revealed that <3.5% (as a ratio of Ag/(Ag + Au), Table S1) of the surface Au atoms had been replaced with Ag. After 20 min of potential cycling, the peak potential had shifted positively by >20 mV, with >10% Ag present at the surface of the Au(111) electrode (Fig. 1c and S2). Further analysis was restricted to electrodes with low extents of Ag–Au alloying on the surface, <3%, such that most of the adsorption sites could be described by three-fold hollow sites coordinated with Au atoms. The peak binding energies for the remaining Ag (368.3 eV) detected in the Ag 3d region were consistent with Ag (368.2 eV) metal rather than Ag^+ (*e.g.* AgCl, 367.4 eV).[28]

The integrated charge in the potential range 0.15–0.39 V and 0.46–0.58 V *vs.* E_{rev} for Cu and Ag, respectively (Fig. 2a, d and S3), was normalized to the theoretical charge density of a full monolayer on Au(111) ($Q^*_{Cu} = -0.44$ mC cm^{-2}, $Q^*_{Ag} = -0.22$ mC cm^{-2}) to estimate metal coverage, θ_M (Fig. 2b, e and eqn (1)).

$$\theta_M(E) = \frac{1}{Q^*_M}\int_{E_i}^{E_f}\frac{j}{\nu}dE \quad (1)$$

At $\nu < 1.0$ V s^{-1} the current response of Ag^+ was linear with ν (Fig. S4) and the peak potential was invariant with ν, both of which are consistent with reversible desorption kinetics. At $\nu >$ 1.0 V s^{-1}, a positive potential shift in the scan-rate-normalized current response was observed. The Cu^{2+} adsorption response began to shift negative at $\nu > 0.25$ V s^{-1}. The apparent rate of metal IIT (r_{app}) was calculated using eqn (2),

$$r_{app} = \frac{|j_M(E)|}{Q^*_M} \quad (2)$$

where $j_M(E)$ is the current density corrected for double layer charging in the absence of either dissolved Cu or Ag. Details on the methods used to correct for double layer charging are available for both species (SI, S2). The dependence of the IIT rate on the surface overpotential, $\xi(E - E_{eq})$—an expression of the difference between the applied electrode potential and the experimentally observed equilibrium potential for a given coverage—was fit to a generalized Butler–Volmer relationship assuming that the charge transferred during the RDS (eqn (3))

$$r_{app} = r_0\theta_M{}^{1-\alpha}(1-\theta_M)^{\alpha}\left(\exp\left[\frac{\alpha e\xi}{k_B T}\right] - \exp\left[\frac{-(1-\alpha)e\xi}{k_B T}\right]\right) \quad (3)$$

where α, e, k_B, T, and r_0 are the transfer coefficient, elementary charge, Boltzmann constant, temperature, and exchange rate, respectively (Fig. 2c and f). This method of analyzing scan-rate-dependent voltammetry data has previously been employed in studies on H adsorption on Pt(111), OH* adsorption on Pt(111), and for Cu adsorption on Au(111).[29–31] For all experimental conditions, the data were well described by assuming a consistent value for α of 0.5.

The exchange rate for Ag IIT increased from 28 to 173 s^{-1} for $[Ag^+] = 1$ to 10 mM, respectively when the total $[ClO_4^-]$ was 0.100 M. A similar trend was observed in electrolytes containing 1.00 M ClO_4^-, with r_0 ranging from 30 to 470 s^{-1} over $[Ag^+] = 1$–10 mM (Fig. S5). The apparent r_0 was constant for $\theta_{Ag} = [0.04$–$0.08]$, suggesting that the kinetic model was appropriate (Fig. S6a). Cu IIT at identical concentrations and coverages yielded more sluggish kinetics, with r_0 ranging from 4 to 35 s^{-1} and from 5 to 70 s^{-1} in 0.100 and 1.00 M ClO_4^-, respectively (Fig. S7).

To understand the interactions between divalent cations and divalent SO_4^{2-}, a common component of metal plating and refining baths, we additionally quantified the adsorption kinetics for Cu^{2+} in H_2SO_4. Cu UPD at Au(111) surfaces in sulfate solutions yielded a characteristic set of peaks associated with two distinct surface phases and a broad, quasireversible region at $E > 0.23$ V *vs.* E_{rev} which was used for kinetic analysis (Fig. S8). The total adsorbed charge prior to kinetically irreversible phase transitions was greater in H_2SO_4 electrolytes and so these samples were used to conduct stripping voltammetry data in a similar manner to Ag (Fig. S9). For $\nu < 3$ V s^{-1} a single peak

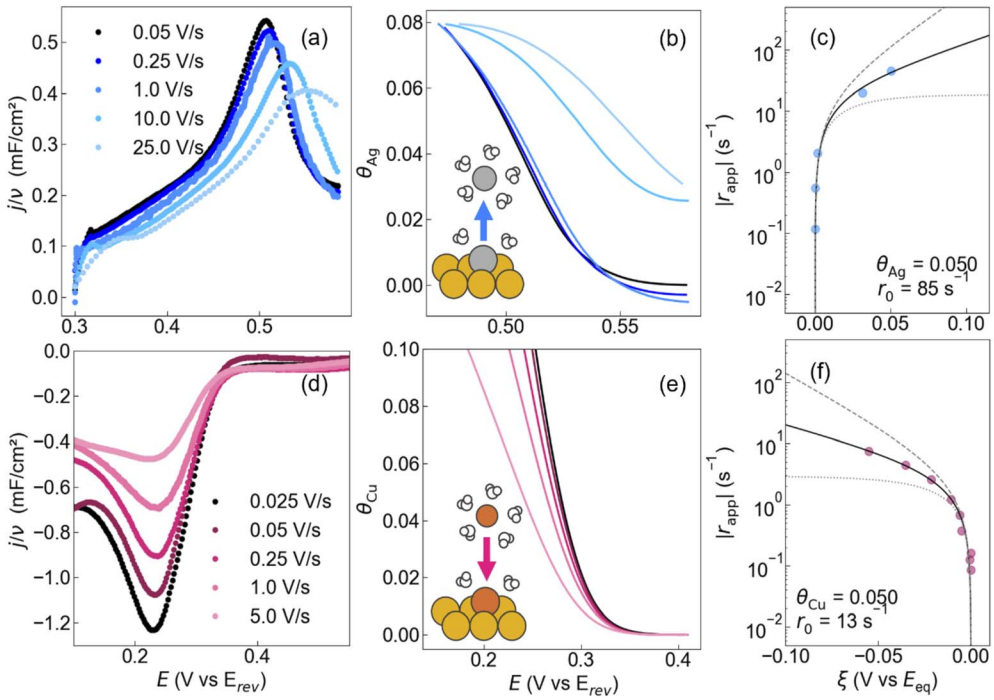

Fig. 2 (a) LSV of Au(111) in 0.003 M $AgClO_4$ and 0.097 M $HClO_4$ (0.100 M ClO_4^-) in the Ag UPD quasireversible region normalized to scan rate (ν = 0.05, 0.25, 1, 10, 25 V s^{-1}). (b) Scan rate dependent Ag coverage (θ_{Ag}). (c) Apparent interfacial ion transfer rate (r_{app}) of Ag^+ as a function of surface overpotential (ξ) at $\theta_{Ag} = 0.05$. Markers represent individual trials and the transfer coefficient, α, was assumed to be 0.5 when fitting the data. Gray dotted and dashed lines represent an alternate fit with $\alpha = 0$ or $\alpha = 1$, respectively. (d) CV of Au(111) in 0.003 M $Cu(ClO_4)_2$ and 0.094 M $HClO_4$ (0.100 M ClO_4^-) in the Cu UPD quasireversible region normalized to scan rate (ν = 0.025, 0.05, 0.25, 1.0, 5.0 V s^{-1}). (e) Cu coverage (θ_{Cu}) as a function of scan rate obtained by integrating the Cu UPD region. (f) r_{app}–ξ behavior for Cu^{2+} at $\theta_{Cu} = 0.05$.

current was observed (Fig. S9a); for $\nu > 10$ V s^{-1} multiple peaks were observed around the potential window where charge equivalent to $\theta_{Cu} = 0.05$ remained on the surface (Fig. S9b). At a surface coverage of 5%, $\theta_{Cu} = 0.05$ and 0.100 M SO_4^{2-}, the exchange rates measured from scans in the adsorption direction (11 ± 2 s^{-1}) and desorption direction (11 ± 4 s^{-1}) were in quantitative agreement (Fig. 3, S6c and S7) and slightly higher than the exchange rates for adsorption measured in 0.100 and 1.00 M ClO_4^- (Fig. S6b and S7).

Both Cu and Ag show an increase in the r_0 as the concentration of the respective metal cation increases as well as a modest relationship between r_0 and the supporting electrolyte concentration (Fig. S5 and S7). The reaction order, m_X, was described by

$$m_X = \partial \log(r_0)/\partial \log([X]) \quad (4)$$

where [X] is the molarity of the species X. The change in r_0 with respect to $[Ag^+]$ is 0.78 ± 0.09 and 1.2 ± 0.07 in 0.10 and 1.00 M ClO_4^-, respectively. Similar m values were measured for Cu^{2+}(aq.): 0.99 ± 0.06 and 1.1 ± 0.1 at the same respective $[ClO_4^-]$ as well as 1.00 M HSO_4^-/SO_4^{2-} (m = 0.80, Fig. 4 and S10). Fig. 5 presents the trend in Cu^{2+} exchange rates for increasing supporting electrolyte concentrations. In solutions containing 1 mM Cu^{2+}, r_0 increased from 1.2 ± 0.5 to 14 ± 0.1 s^{-1} when the concentration of $HClO_4$(aq.) increased from 0.010 to 10.0 M $HClO_4$(aq.) (Fig. 5). The m_{HClO_4} was 0.33, indicating that increased supporting electrolyte concentrations led to a moderate, positive impact on Cu^{2+} IIT kinetics. However, similar experiments in H_2SO_4(aq.) electrolytes yielded increased r_0 at low $[SO_4^{2-}]$ and $m_{H_2SO_4}$ (0.05) was inconsistent with an electrolyte concentration effect, indicating that the identity of the supporting anion is dominant relative to H_3O^+. At increased concentrations of H_2SO_4, the initial stages of Cu adsorption were no longer kinetically reversible, and a phase transition occurred prior to $\theta_{Cu} = 0.05$ (Fig. S11).

The double layer structure for Au(111)/Cu surfaces was studied by fitting the θ_{Cu}–E relationship for Cu^{2+} to adsorption isotherms for various $[Cu^{2+}]$ and $[ClO_4^-]$. A scan rate of ν = 25 mV s^{-1} during cyclic voltammetry was sufficiently slow such that $E(\theta_{Cu})$ varied by less than 5 mV with a doubling of ν. These data were fit to a Frumkin θ–E isotherm

$$E = E_{1/2} + \frac{RT}{F}\left(-\ln[C_A]/n + \ln\left[\frac{\theta}{1-\theta}\right] + g\left[\theta - \frac{1}{2}\right]\right) \quad (5)$$

where $E_{1/2}$, R, F, C_A, n, and g are the potential of half coverage, the universal gas constant, Faraday's constant, bulk concentration of the dissolved transition metal, the number of charges per adsorbate, and the adsorbate–adsorbate interaction parameter, respectively. A positive value for g indicates unfavorable adsorbate interactions and has been related to the free energy of interactions between adsorbed species, γ, by $g = 2\gamma/RT$.[32] When g is zero, the equation for a potential-dependent Langmuir isotherm is recovered.

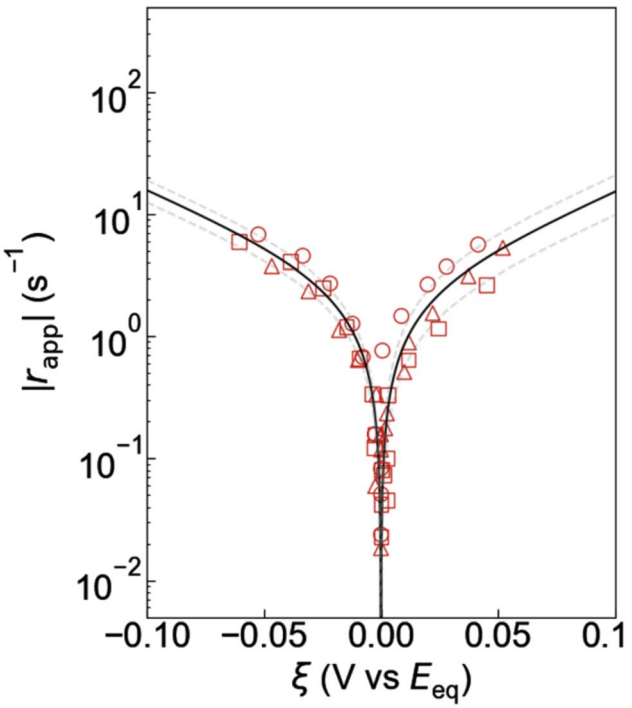

Fig. 3 The apparent interfacial ion transfer rate (r_{app}) for 0.001 M Cu^{2+} in 0.100 M SO_4^{2-} as a function of ξ at $\theta_{Cu} = 0.05$. Each set of symbols represents one experiment in which both adsorption and desorption experiments were performed in the same cell with the same electrodes. The different markers represent the experimental repeats. The solid black line represents the averaged line of best fit, and the grey dashed lines represent one standard deviations of the fit.

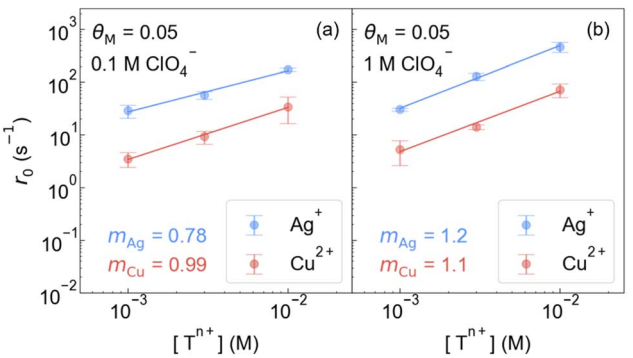

Fig. 4 Equilibrium exchange rate (r_0) of metal cations *versus* the concentration of the respective metal cation ([X] = 1.0 mM, 3.0 mM, 10.0 mM), measured at 5% coverage. (a) The exchange rates for Ag^+ (blue) and Cu^{2+} (orange) in 0.1 M ClO_4^-. (b) The exchange rates for Ag^+ (blue) and Cu^{2+} (orange) in 1 M ClO_4^-. Circles represent experimental data, with the error bars representing the standard deviations across three separate trials. The solid-colored lines represent the reaction order of the rates with respect to concentration. (X = Ag^+ or Cu^{2+}). The apparent reaction order, m, was measured from the slope $\partial \log(r_0)/\partial \log([X])$.

Cu^{2+} adsorbed onto Au(111) surfaces exhibited a positive g for all concentrations of $HClO_4$. In dilute (1.0 mM) Cu^{2+} and the supporting electrolyte (10 mM ClO_4^-), g was 13 ± 4 (Fig. S12)

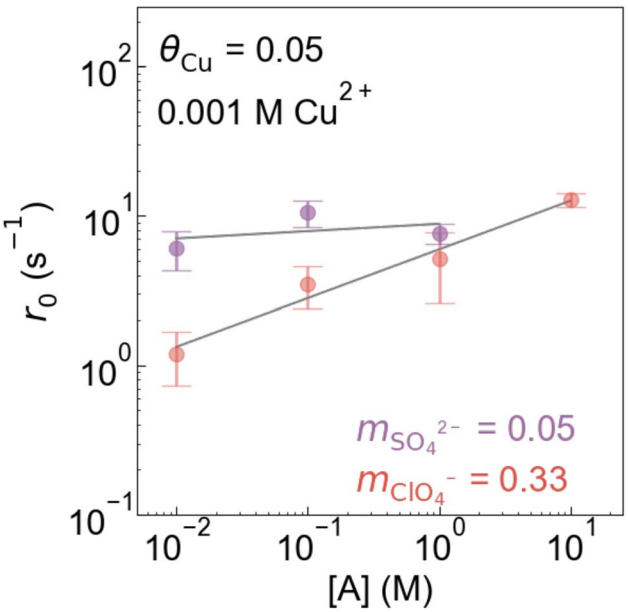

Fig. 5 Dependence of the equilibrium exchange rate (r_0) of the metal cation *vs.* the concentration of supporting anions ([A]) at 5% coverage. The light orange dots are perchlorate at [ClO_4^-] = 0.01, 0.10, 100, and 10 M. The purple dots are sulfate at [SO_4^{2-}] = 0.01, 0.1, and 1 M. The circle symbols represent experimental data, with the error bars representing the standard deviations. The grey line represents the reaction order, m, with respect to the supporting anion concentration.

and decreased with increasing [ClO_4^-] to 6.6 ± 0.6 and 2.9 ± 0.1 for 100 mM (Fig. S13) and 1.00 M solutions (Fig. S14), respectively. The average g for at least two independent measurements/electrode surfaces was generally insensitive to increasing [Cu^{2+}] and varied from 2.9 to 3.6 in [ClO_4^-] = 0.100 M (Fig. S15), although the apparent $E_{1/2}$ *versus* E_{rev} shifted positively up to 80 mV. Thus, although the interaction energies between adsorbed Cu^{2+} were insensitive to the bulk [Cu^{2+}] (Fig. S15a), they trended towards zero as the supporting electrolyte concentration was increased (Fig. S15b).

It is possible that Ag^+ and Cu^{2+} promote adsorption by modifying the electric field more strongly than the supporting H_3O^+ cations,[33] and so we investigated the impact of supporting alkali cations *via* additions of K^+ to SO_4^{2-} electrolytes during adsorption of Cu^{2+}. Sulfate electrolytes were selected for this analysis because they conveniently lacked a strong anion concentration effect. The presence of K^+ led to an increased peak cathodic current relative to electrolytes where K^+ was absent (Fig. S16a). K^+ had a substantial effect on the critical coverage of adsorbed Cu^{*z+} prior to the sharp current onset associated with a surface phase transition; however, K^+ did not appear to impact the θ–E behavior at more positive potentials compared to K-free electrolytes (Fig. S16b). The exchange rate of Cu^{2+} at $\theta > 0.05$ and in the presence of K^+ was within experimental error of K^+-free electrolytes (Fig. S17).

Aqueous Cu^{2+} catalyzes the decomposition of ClO_4^- to Cl^- within weeks, and the presence of low concentrations (<1 μM) of Cl^- is likely to influence the kinetics of both Ag and Cu deposition.[25] To avoid any possible Cl^- contamination all Cu^{2+}

solutions were tested within a week of preparation. A commensurate pair of minor, sharp peaks were noted in the reversible region of Cu^{2+} adsorption in aged $Cu(ClO_4)_2$ solutions (Fig. S18), and we attribute these to the presence of Cl^-. Electrolytes which exhibited these peaks were considered to be Cl^- contaminated and were not used in the kinetic analysis.

Discussion

Quasireversible adsorption of Ag and Cu on Au(111) electrodes allowed for direct measurements of interfacial ion transfer kinetics at a site-defined metal surface and in the absence of first-order phase transitions (Fig. 1). Here, we have specifically focused on low (5%) coverages of adsorbates to maximize the contribution of isolated Au(111) adsorption sites to the measured faradaic response. Assuming that Ag and Cu were randomly distributed across three-fold hollow sites and that the contribution from step-edges and grain boundaries is negligible, the probability of the next adsorption site being free of nearest neighbor is >90% when $\theta < 0.01$ but falls to <60% when $\theta > 0.05$ (SI, S2). Careful consideration and control of θ is thus essential for an atomistic understanding of metal IIT, and this quantity is rarely controlled during the deposition/corrosion of bulk metals. Measurements of UPD kinetics at low coverages may thus serve as a privileged model for site-specific charge transfer kinetics associated with these reactions. Similar adatoms are believed to be present during bulk deposition and corrosion. Gerischer reported the surface concentration of Ag adatoms to be $\sim 10^{13}/cm^{-2}$, equivalent to 2–4% coverage, whereas Despic reported much greater concentrations of surface charge for Cu electrodes, equivalent to $\sim 3 \times 10^{15}/cm^{-2}$, indicating the presence of a roughened surface and hindering the ability to estimate the coverage of adsorbates.[34,35] The reaction orders and turnover frequencies measured in this work are most pertinent to corrosion and deposition at low applied bias, when the coverage of adatoms is the lowest.

The exchange rate for Ag at Au(111) is 2–6 times faster than the exchange rate for Cu independent of $[Cu^{2+}]$. The average standard rate constants for charge transfer, k^0, are reported in Table 1 and for Ag IIT in 1 M ClO_4^- are within one order of magnitude of some adiabatic electron transfer reactions (0.85 ± 0.2 cm s^{-1}).[36] The reported exchange rates for both Ag^+ and Cu^{2+} vary widely, presumably due to differences in surface preparation and the geometric density of active sites. Reported Cu^{2+} exchange current densities vary by an order of magnitude, from $0.4–4 \times 10^{-2}$ A cm^{-2} in 5 mM $CuSO_4$, with asymmetric transfer coefficients for the anodic and cathodic reactions.[37] Ag^+ exchange current densities vary wider still, based on electrode preparation and Ag^+ concentration, but the value measured here (6×10^{-3} A cm^{-2}) for elementary Ag IIT at 1 mM Ag^+ is slower than what has previously been reported for polycrystalline Ag surfaces (1.5×10^{-1} A cm^{-2}) at similar concentrations,[38,39] suggesting that reported rates of Ag/Ag^+ exchange are convoluted by a large, albeit unknown, number of active sites. Here, we report a symmetric $\alpha = 0.5$ for elementary Cu^{2+} IIT, with a consistent standard rate constant of 1×10^{-2} cm s^{-1} at 5% surface coverage across varied electrolytes identities, ionic strengths, as well as $a_{Cu^{2+}}$. Notably, this value is within the range of reported rate constants for Cu^{2+} amalgamation ($1–5 \times 10^{-2}$ cm s^{-1}),[40] which serves as a similar model system for elementary IIT albeit where the concentration/surface excess of the adsorbed product is unknown.

Table 1 Comparison of standard rate constants for interfacial ion transfer of Ag^+ and Cu^{2+} at Au(111) in 0.10 M and 1 M $HClO_4$ at 20 °C

	k^0 (cm s^{-1}) (0.10 M ClO_4^-)	k^0 (cm s^{-1}) (1.00 M ClO_4^-)
Cu^{2+}	$8(2) \times 10^{-3}$	$1.3(3) \times 10^{-2}$
Ag^+	$5.0(6) \times 10^{-2}$	$9.2(8) \times 10^{-2}$

The reaction order for IIT exchange rates can be used to resolve microscopic steps associated with ion transfer. A unique aspect of adsorption/desorption reactions is that activity of the product cannot be controlled independently of the applied potential. Prior studies on adsorption at Pt(111) surfaces have reported a reaction order of 0.5 with respect to H_3O^+ for hydride adsorption limited by proton-coupled-electron transfer, whereas the hydride adsorption from H_2O exhibits a 0^{th} order dependence with respect to OH^- activity in alkaline media, implying that this process includes a chemically distinct rate determining step.[29] Both OH^- and H^+ adsorption kinetics exhibit a stronger dependence on the concentration of supporting alkali cations, such as Na^+, with $m_{Na^+} \sim 1$ reported for Pt(111) at pH ~ 13. Here, we report that site-isolated transition metal, T, adsorption (eqn (6))

$$T_{aq.}{}^{n+} + * + ne^- \leftrightarrow T* \quad (6)$$

exhibits a consistent $\alpha \sim 0.5$ but $m \sim 2\alpha$ for both a monovalent and divalent transition metal cation. Generally, the measured m was ≥ 1 but for Ag^+ adsorption in 0.10 M ClO_4^- and Cu^{2+} adsorption in 1.0 M SO_4^{2-}, m was 0.78 ± 0.09 and 0.8 ± 0.2, respectively (Fig. 4 and S10). We interpret these results to be generally consistent with, $m_{T^+} \sim 2\alpha$ and $0.4 < \alpha < 0.6$,[32] which would be consistent with a single elementary charge transfer step but alludes to a more complex path for desolvation of aqueous transition metals (SI, S3–S8).

The analysis for the self-exchange of Ag/Ag^+, which does not require analysis of multiple charge transfer steps, provides a foundation for understanding metal IIT. The increased reaction order with respect to Ag^+ is consistent with a general promoting effect of dissolved transition metal and this could be caused by specific intermolecular interactions or changes in the local electric field at the adsorption site. For example, multistep mechanisms that include a bimolecular reaction between Ag^+(aq.) prior to the rate determining adsorption step may result in the measured $m_{Ag^+} = 2\alpha$ (*e.g.* $2Ag^+ \leftrightarrow Ag_a{}^+ + Ag_b{}^+$) provided that the activity of both species are not linked by a simple mole balance. We hypothesize that this step could be related to solvent exchange leading to an undercoordinated Ag^+ species which is able to more closely approach the adsorption site where charge transfer occurs (eqn (7) and (S20)–(S26))

$$2Ag^+(H_2O)_n \leftrightarrow Ag^+(H_2O)_{n+1} + Ag^+(H_2O)_{n-1} \quad (7)$$

Previously calculated trajectories of individual Ag^+ deposition at model Ag surfaces indicate the presence of a pre-associated species within the inner Helmholtz plane, and later trajectories for Zn^{2+} deposition which include nonlinear solvent coupling terms further support an inner sphere pathway.[12,41] In the case of silver, these results suggest that the formation of this species could be promoted by proximal, spectator Ag^+ cations. This case can easily be distinguished from a mechanism involving an adsorbed $Ag^{0/+}$ species acting as a promoter based on the coverage dependence of the reaction. However, the effects of pre-adsorption without charge transfer and the role of non-ideal interactions between adsorbates or the transition state are not distinguishable from the more general mechanism, based on differences in the exchange rate and transfer coefficient alone (eqn (S27)–(S38)). The complex relationship between m_{T^+} and α may also be explained by transition metal cations exerting a generalized cation effect by modifying the electric field at the site of transfer or by impacting the rigidity of the solvent within the double layer.[42]

A similar analysis conducted for $Cu^{+/2+}$ exchange is consistent with the general presence of metal-cation promoted transfer which may be described by a bimolecular reaction prior to charge transfer, here represented as solvent exchange (eqn (8)).

$$2Cu^{2+}(H_2O)_n \leftrightarrow Cu^{2+}(H_2O)_{n+1} + Cu^{2+}(H_2O)_{n-1} \quad (8)$$

We do not rule out the possibility of an alternate mechanism for metal cations to promote self-exchange, as a more comprehensive study of interactions with supporting metal cations is required. Although the reported $m_{Cu^{2+}}$ and α for Cu^{2+} vary widely based on electrolyte and electrode preparation,[37] Cu^{2+} deposition is generally believed to proceed *via* two distinct charge transfer steps, with the formation of unstable aqueous Cu^+ species being rate-determining. During these UPD measurements, outer-sphere electron transfer to $Cu^{+/2+}$ is unlikely, as the formal potential for the reaction is >200 mV negative of the electrochemical potentials used to quantify Cu* exchange. Nevertheless, accounting for possible differences in the density of adsorption sites, the exchange currents measured for self-exchange of Cu^{2+} at Au(111) surfaces are generally in accord with previously reported values for overall Cu/Cu^{2+} exchange, suggesting that the coupled ion–electron transfer step quantified here, rather than homogeneous electron transfer to an aqueous Cu^{2+} species or chemical adsorption of Cu^{2+} prior to electron transfer, is an enabling step for the rapid kinetics of Cu deposition, generalized as eqn (9).

$$Cu^{2+} + e^- + * \leftrightarrow Cu^+* \quad (9)$$

Differences in the observed rate constants for Ag^+ adsorption and Cu^{2+} adsorption are more often attributed to chemical properties of the solvated metal cation, rather than the properties of the adsorbed $Cu^{0/+}$ or $Ag^{0/+}$ species. While the reorganization energy of the solvent is likely associated with a desolvation step, previously measured exchange rates for metal plating, as well as those measured here for IIT, are inconsistent with a transition state barrier that scales with the total solvation enthalpy.[11] Notably, despite a roughly four-fold difference between the solvation enthalpies of monovalent and divalent cations (5 eV and 20 eV respectively),[12,18] the exchange rates of Ag^+ and Cu^{2+} at Au(111) differ only by a factor of two in 0.10 M $HClO_4$. This suggests that the bulk solvation enthalpy is a poor descriptor for the reorganization energy associated with the rate determining step of transition metal IIT. These data strengthen the argument that most of the enthalpy of desolvation associated with a metal deposition or corrosion reaction occurs before/after the rate determining step. The approach distance of the monovalent cation is expected to be less than that of the divalent cation, as calculated for Zn^{2+} and Zn^+ at Zn metal surfaces,[16] but this apparently does not directly influence the apparent α. Inspired by recent simulations of Zn/Zn^{2+} deposition, we hypothesize that the greater approach distance for the solvated Cu^{2+} species leads to weaker coupling and the more sluggish IIT kinetics in comparison to Ag^+.[43]

The weakly positive correlation between IIT kinetics and increasing perchloric acid concentration is consistent with increased screening effects in the double layer and/or decreasing rigidity of the double layer with increasing ionic strength.[30] Near-surface anions support a greater surface excess of cations and thereby increase the local concentration of reactants prior to desolvation and ion transfer. These effects are also evident in the θ–E response, which provides surface-sensitive information about changes to the adsorbate environment in response to changes in the bulk electrolyte (Fig. S15b). The apparent g for adsorbed Cu at Au(111) was insensitive to the concentration of Cu^{2+} but was weakly influenced by the concentration of $HClO_4$, indicating less repulsive interactions between surface cations. A decrease in g could be caused by a combination of increased screening effects with higher ionic strength and/or the increased anion concentration disrupting interactions between interfacial water molecules.[30]

Whereas perchlorate lacks an ordered adsorption phase and exhibits a lower capacitance in the potential window used for kinetic analysis (Fig. S19), sulfate anions form an ordered layer ($\theta = 0.20$) on Au(111),[44,45] and a disordered layer has been observed at concentrations > 5 M.[46] The zeroth-order anion effect for sulfate at Au(111) stands in contrast to the positive anion effect for perchlorate, and is consistent with a relatively stable Γ_{SO_4} with increasing $a_{H_2SO_4}$ for pH ≥ 0. The presence of K^+ in sulfate-containing electrolytes did not lead to a change in the apparent interaction parameter at low coverages. However, K^+ cations did contribute to a positive shift in the peak potential which was caused by a lesser integrated charge prior to the sharp change in current assigned to a surface phase transition (Fig. S16b). This suggests that although K^+ cations do not impact the stability of Cu adsorbates at low coverages, they induce a transition to an ordered surface layer at a lower Cu coverage, likely because they contribute to the total excess charge within the double layer region.

No differences in metal IIT were observed in response to a change in the bulk a_{H_2O}. The reported a_{H_2O} in 10 M $HClO_4$(aq.) and 10 M H_2SO_4(aq.) is 0.03 and 0.045, respectively,[47,48] but the exchange rate for Cu^{2+} was consistent across a wide range of

[H_2SO_4] and exhibited a similar m_{HClO_4} at low and high concentrations of $HClO_4$. Uncoordinated water is a necessary product of the overall deposition of aqueous transition metals, and this result implies that either the surface activity of H_2O is relatively insensitive to changes in the bulk activity or else uncoordinated H_2O is not a participant in the rate determining step for Cu^{2+} IIT. This is significant for understanding the behavior of metal plating and ion insertion reactions in "water-in-salt" electrolytes and suggests that there is a significant barrier to modifying the solvent activity without changes to the electrode surface environment itself.[49,50]

A few experimental barriers to measuring isolated steps of deposition/corrosion have been mitigated here through the use of freshly prepared Au(111) surfaces and Cu^{2+} electrolytes prepared from high purity oxides. Investigations of Ag UPD at Au surfaces are limited in part due to the tendency of Ag to alloy with the substrate, leading to a time-varying and irreproducible electrochemical response.[23] Au(111) surfaces exhibited changes in electrochemical response after less than 30 min of exposure (Fig. 1c), whereas frequent replacement of Au(111)-textured thin film electrodes allowed for reproducible measurements of Ag desorption kinetics without the apparent influence of Ag/Au surface alloys that would not be possible with traditional Au(111) solid electrodes (Fig. 4). The positive shift in the Ag desorption peak implies more favorable Ag/Au interactions that could be caused by an increase in vacancies, pits, and step edges serving as active sites. As the extent of Ag/Au alloying increases, the number of active sites for Ag UPD decreases, which would lead to an overestimation of the active sites and an underestimation of the apparent rate and exchange rate. Furthermore, the electronic properties of the adsorption sites will be modified after the formation of a near-surface alloy and this could be reflected in the changing onset potential for desorption (Fig. 1c).

Future studies of metal IIT should investigate the chemical principles required to predict rate constants for metal adsorption, including the electronic structure of metal cations and the coordination environment of the adsorption site. Studies on the temperature dependence and supporting cation identity may further clarify how solvent transfer and reorganization influence the rate of IIT, which would provide design principles for accelerated deposition or suppressed corrosion. Additionally, the methodology to measure exchange rates for controlled metal adsorbates could shed light on the molecular mechanisms of additives used for Cu deposition in semiconductor interconnects, increasing charge/discharge rates in redox-flow battery electrolytes, and the industrial electrowinning and electrorefining process of energy-critical metals.

Conclusions

Underpotential deposition of Cu^{2+} and Ag^+ at well-defined Au(111) interfaces served to isolate a microscopically reversible step involved in metal corrosion and deposition and enabled a controlled kinetic analysis of self-exchange during interfacial ion transfer. This system addresses two limitations of traditional kinetic measurements at growing/corroding metal surfaces: (1) the coverage of adsorbates is not known and (2) both the number density and identity of active sites are poorly defined. The standard rate constant for Ag^+ IIT at Au(111) was within an order of magnitude of the reported adiabatic electron transfer for $Ru(NH_3)_6$ and the exchange rate of Cu^{2+} was consistently within an order of magnitude of that measured for Ag^+. The coverage dependence and transfer coefficient associated with adsorption/desorption of both Ag^+ and Cu^{2+} suggest that a coupled ion–electron transfer step was the rate determining step for adsorption/desorption. The self-exchange rate with respect to the metal cation concentration was quantified at a constant coverage of adsorbates and was ~1 for both Cu^{2+} and Ag^+; this could be described by a multi-step mechanism involving biomolecular interactions between free cations prior to transfer. A mechanism involving solvent transfer prior to adsorption/desorption was proposed to fit this mechanism and is consistent with zeroth-order kinetics with respect to bulk H_2O. A positive anion effect was observed in perchlorate but not in sulfate electrolytes, with the latter exhibiting increased exchange rates at lower ionic strengths.

Author contributions

E. I. S.: conceptualization, methodology, investigation, visualization, writing – original draft, review, & editing; K. A. T.: methodology, investigation, visualization, writing – review & editing; F. B. S.: investigation, writing – review & editing; P. A. K.: supervision, visualization, writing – original draft, review, & editing.

Conflicts of interest

There are no conflicts to declare.

Data availability

Additional data supporting this article have been included as part of the supplementary information (SI). Supplementary information: eqn (S1)–(S56), Fig. S1–S19 and Table S1, a detailed derivation of kinetic models, X-ray diffraction of annealed Au thin films, high resolution XPS data for annealed Au electrodes before and after exposure to Ag^+, additional electrochemical data and measured exchange rates in concentrated H_2SO_4 and solutions containing K^+. See DOI: https://doi.org/10.1039/d6sc00974c.

Unprocessed electrochemical data are available at https://github.com/Kempler-Group/CuAgUPD2026.

Acknowledgements

This material is based on work performed by the Liquid Sunlight Alliance, which is supported by the U.S. Department of Energy, Office of Science, Office of Basic Energy Sciences, Fuels from Sunlight Hub under Award Number DE-SC0021266. We thank Shannon W. Boettcher and Jin Suntivich for valuable scientific discussions on interfacial ion transfer kinetics.

Notes and references

1 P. C. Andricacos, C. Uzoh, J. O. Dukovic, J. Horkans and H. Deligianni, Damascene Copper Electroplating for Chip Interconnections, *IBM J. Res. Dev.*, 1998, **42**(5), 567–574, DOI: 10.1147/rd.425.0567.

2 J. K. Jhothiraman and R. Balachandran, Electroplating: Applications in the Semiconductor Industry, *Adv. Chem. Eng. Sci.*, 2019, **9**(2), 239–261, DOI: 10.4236/aces.2019.92018.

3 *Copper Plating Solutions for Semiconductor Manufacturing Market Growth Analysis, Market Dynamics, Key Players and Innovations, Outlook and Forecast 2025-2031*, Intelmarketresearch, accessed 2025-04-17, https://www.intelmarketresearch.com/chemicals-and-materials/375/copper-plating-solutions-semiconductor.

4 E. Gileadi, Problems in Interfacial Electrochemistry That Have Been Swept under the Carpet, *J. Solid State Electrochem.*, 2011, **15**(7–8), 1359–1371, DOI: 10.1007/s10008-011-1344-5.

5 N. B. Lewis, J. Kelly, J. G. Gardner, N. K. Razdan, S. Ardo, T. E. Markland and Y. Surendranath, Ion-Exchange-Mediated Pre-Association Gates Interfacial PCET, *Chem*, 2026, **12**(3), 102813, DOI: 10.1016/j.chempr.2025.102813.

6 N. D'Antona, J. Kelly, N. Barnard, S. Ardo, Y. Wang, Y. Surendranath, T. E. Markland, P. A. Kempler and S. W. Boettcher, Proton-Transfer Kinetics at Liquid–Liquid Interfaces, *J. Am. Chem. Soc.*, 2025, **147**(25), 21408–21418, DOI: 10.1021/jacs.4c18349.

7 D. Tang, N. Keyes, J. C. Rose, J. E. Gonzales, M. Yang, M. D. Giles, Y. Surendranath, S. Ardo and M. B. Minus, Synthesis of 4,5-Disubstituted *o* -Phenylenediamines: An Enabling Platform for Electrochemical Investigations of Interfacial Ion Transfer Reactions, *J. Org. Chem.*, 2025, 5c00538, DOI: 10.1021/acs.joc.5c00538.

8 Y. Zhang, D. Fraggedakis, T. Gao, S. Pathak, D. Zhuang, C. Grosu, Y. Samantaray, A. R. C. Neto, S. R. Duggirala, B. Huang, Y. G. Zhu, L. Giordano, R. Tatara, H. Agarwal, R. M. Stephens, M. Z. Bazant and Y. Shao-Horn, Lithium-Ion Intercalation by Coupled Ion-Electron Transfer, *Science*, 2025, **390**(6768), eadq2541, DOI: 10.1126/science.adq2541.

9 C. E. D. Chidsey, Free Energy and Temperature Dependence of Electron Transfer at the Metal-Electrolyte Interface, *Science*, 1991, **251**(4996), 919–922, DOI: 10.1126/science.251.4996.919.

10 B. E. Conway and J. O. Bockris, The Mechanism of Electrolytic Metal Deposition, *Proc. R. Soc. Lond., Ser. A Math. Phys. Sci.*, 1997, **248**(1254), 394–403, DOI: 10.1098/rspa.1958.0251.

11 E. Gileadi, The Enigma of Metal Deposition, *J. Electroanal. Chem.*, 2011, **660**(2), 247–253, DOI: 10.1016/j.jelechem.2011.01.025.

12 L. M. C. Pinto, E. Spohr, P. Quaino, E. Santos and W. Schmickler, Why Silver Deposition Is so Fast: Solving the Enigma of Metal Deposition, *Angew. Chem., Int. Ed.*, 2013, **52**(30), 7883–7885, DOI: 10.1002/anie.201301998.

13 R. Kang, Y. Zhao, D. Hait, J. A. Gauthier, P. A. Kempler, K. A. Thurman, S. W. Boettcher and M. Head-Gordon, Understanding Ion-Transfer Reactions in Silver Electrodissolution and Electrodeposition from First-Principles Calculations and Experiments, *Chem. Sci.*, 2024, **15**(13), 4996–5008, DOI: 10.1039/D3SC05791G.

14 M. Darvas, M. Jorge, M. N. D. S. Cordeiro, S. S. Kantorovich, M. Sega and P. Jedlovszky, Calculation of the Intrinsic Solvation Free Energy Profile of an Ionic Penetrant Across a Liquid–Liquid Interface with Computer Simulations, *J. Phys. Chem. B*, 2013, **117**(50), 16148–16156, DOI: 10.1021/jp404699t.

15 P. Clabaut, B. Schweitzer, A. W. Götz, C. Michel and S. N. Steinmann, Solvation Free Energies and Adsorption Energies at the Metal/Water Interface from Hybrid Quantum-Mechanical/Molecular Mechanics Simulations, *J. Chem. Theory Comput.*, 2020, **16**(10), 6539–6549, DOI: 10.1021/acs.jctc.0c00632.

16 O. Pecina and W. Schmickler, The Solvent Influence on the Electrochemical Transfer of Divalent Ions, *Chem. Phys.*, 2000, **252**(3), 349–357, DOI: 10.1016/S0301-0104(99)00332-8.

17 O. Pecina, W. Schmickler and E. Spohr, On the Mechanism of Electrochemical Ion Transfer Reactions, *J. Electroanal. Chem.*, 1995, **394**(1–2), 29–34, DOI: 10.1016/0022-0728(95)92838-O.

18 M. Uudsemaa and T. Tamm, Calculation of Hydration Enthalpies of Aqueous Transition Metal Cations Using Two Coordination Shells and Central Ion Substitution, *Chem. Phys. Lett.*, 2004, **400**(1), 54–58, DOI: 10.1016/j.cplett.2004.10.082.

19 M. H. Hölzle, V. Zwing and D. M. Kolb, The Influence of Steps on the Deposition of Cu onto Au(111), *Electrochim. Acta*, 1995, **40**(10), 1237–1247, DOI: 10.1016/0013-4686(95)00055-J.

20 M. H. Hölzle, U. Retter and D. M. Kolb, The Kinetics of Structural Changes in Cu Adlayers on Au(111), *J. Electroanal. Chem.*, 1994, **371**(1), 101–109, DOI: 10.1016/0022-0728(93)03235-H.

21 E. Herrero, L. J. Buller and H. D. Abruña, Underpotential Deposition at Single Crystal Surfaces of Au, Pt, Ag and Other Materials, *Chem. Rev.*, 2001, **101**(7), 1897–1930, DOI: 10.1021/cr9600363.

22 E. Herrero and H. D. Abruña, Underpotential Deposition of Mercury on Au(111): Electrochemical Studies and Comparison with Structural Investigations, *Langmuir*, 1997, **13**(16), 4446–4453, DOI: 10.1021/la970109t.

23 C. M. Whelan, M. R. Smyth, C. J. Barnes, G. A. Attard and X. Yang, Surface Structural Transitions Induced by Repetitive Underpotential Deposition of Ag on Au(111), *J. Electroanal. Chem.*, 1999, **474**(2), 138–146, DOI: 10.1016/S0022-0728(99)00320-4.

24 D. Krznarić and T. Goričnik, Reactions of Copper on the Au(111) Surface in the Underpotential Deposition Region from Chloride Solutions, *Langmuir*, 2001, **17**(14), 4347–4351, DOI: 10.1021/la001562z.

25 J. Hotlos, O. M. Magnussen and R. J. Behm, Effect of Trace Amounts of C1- in Cu Underpotential Deposition on

Au(Lll)in Perchlorate Solutions: An in-Situ Scanning Tunneling Microscopy Study, *Surf. Sci.*, 1995, 129–144.

26 K. Ogaki and K. Itaya, In Situ Scanning Tunneling Microscopy of Underpotential and Bulk Deposition of Silver on Gold (111), *Electrochim. Acta*, 1995, **40**(10), 1249–1257, DOI: 10.1016/0013-4686(95)99706-2.

27 I. Park and H. Baltruschat, In Situ Friction Study of Ag Underpotential Deposition (UPD) on Au(111) in Aqueous Electrolyte, *ChemPhysChem*, 2021, **22**(10), 952–959, DOI: 10.1002/cphc.202100130.

28 M. Nehal, F. El, A. Bouzidi, A. Nakrela, R. Miloua, M. Medles, R. Desfeux, J.-F. Blach, P. Simon and M. Huvé, Synthesis and Characterization of Antireflective Ag@AgCl Nanocomposite Thin Films, *Optik*, 2020, **224**, 165568, DOI: 10.1016/j.ijleo.2020.165568.

29 D.-Y. Kuo, X. Lu, B. Hu, H. D. Abruña and J. Suntivich, Rate and Mechanism of Electrochemical Formation of Surface-Bound Hydrogen on Pt(111) Single Crystals, *J. Phys. Chem. Lett.*, 2022, **13**(27), 6383–6390, DOI: 10.1021/acs.jpclett.2c01734.

30 C.-Y. Lin, H. D. Abruña and J. Suntivich, Cations Affect Water Activation on Pt(111) in Alkaline Media, *J. Electrochem. Soc.*, 2025, **172**(1), 016503, DOI: 10.1149/1945-7111/ada7a3.

31 K. A. Thurman, C. M. Cannan, R. Shekhar, Y. Zhao, S. W. Boettcher and P. A. Kempler, Anions in Corrosion: Influence of Polymer Electrolytes on the Interfacial Ion Transfer Kinetics of Cu at Au(111) Surfaces, *ACS Electrochem.*, 2025, **1**(4), 425–432, DOI: 10.1021/acselectrochem.4c00181.

32 A. J. Bard, L. R. Faulkner and H. S. White, *Electrochemical Methods*, 2022.

33 M. C. O. Monteiro, F. Dattila, B. Hagedoorn, R. Garcia-Muelas, N. Lopez and M. T. M. Koper, Absence of CO2 Electroreduction on Copper, Gold and Silver Electrodes without Metal Cations in Solution, *Nat. Catal.*, 2021, **4**, 654–662.

34 A. R. Despić, Deposition and Dissolution of Metals and Alloys. Part B: Mechanisms, Kinetics, Texture, and Morphology, in *Comprehensive Treatise of Electrochemistry: Volume 7 Kinetics and Mechanisms of Electrode Processes*, ed. B. E. Conway, J. O. Bockris, E. Yeager, S. U. M. Khan and White R. E., Springer US, Boston, MA, 1983, pp. 451–528, DOI: 10.1007/978-1-4613-3584-9_8.

35 H. Gerischer, On the Mechanism of Electrolytic Deposition and Dissolution of Solid Metals II. Galvanostatic Switching-On Processes at Silver Electrodes and the Kinetics of Crystal Growth, *Journal of Electrochemistry, Reports of the Bunsen Society for Physical Chemistry*, 1958, **62**(3), 256–264, DOI: 10.1002/bbpc.19580620308.

36 E. Santos, T. Iwasita and W. Vielstich, On the Use of the Coulostatic Method for the Investigation of Fast Redox Systems, *Electrochim. Acta*, 1986, **31**(4), 431–437, DOI: 10.1016/0013-4686(86)80105-0.

37 A. R. Despić, Deposition and Dissolution of Metals and Alloys. Part B: Mechanisms, Kinetics, Texture, and Morphology, in *Comprehensive Treatise of Electrochemistry*, ed. B. E. Conway, J. O. Bockris, E. Yeager, S. U. M. Khan and R. E. White, Springer US, Boston, MA, 1983, pp. 451–528, DOI: 10.1007/978-1-4613-3584-9_8.

38 H. Gerischer, Models for the Discussion of the Photo-Electrochemical Response of Oxide Layers on Metals, *Corros. Sci.*, 1989, **29**, 257–266.

39 D. Larkin and N. Hackerman, The Ag+-Ag Exchange Reaction in Aqueous Acidic Nitrate Electrolyte, *J. Electrochem. Soc.*, 1977, **124**(3), 360.

40 J. E. B. Randles and K. W. Somerton, Kinetics of Rapid Electrode Reactions. Part 4.—Metal Ion Exchange Reaction at Amalgam Electrodes, *Trans. Faraday Soc.*, 1952, **48**, 951–955.

41 P. Quaino, E. Colombo, F. Juarez, E. Santos, G. Belletti, A. Groß and W. Schmickler, On the First Step in Zinc Deposition – A Case of Nonlinear Coupling with the Solvent, *Electrochem. Commun.*, 2021, **122**, 106876, DOI: 10.1016/j.elecom.2020.106876.

42 J. Resasco, A Universal Model of Cation Effects in Electrocatalysis, *JACS Au*, 2025, **5**(11), 5253–5266, DOI: 10.1021/jacsau.5c01115.

43 P. Quaino, E. Colombo, F. Juarez, E. Santos, G. Belletti, A. Groß and W. Schmickler, On the First Step in Zinc Deposition – A Case of Nonlinear Coupling with the Solvent, *Electrochem. Commun.*, 2021, **122**, 106876, DOI: 10.1016/j.elecom.2020.106876.

44 F. Hausen, N. N. Gosvami and R. Bennewitz, Anion Adsorption and Atomic Friction on Au(111), *Electrochim. Acta*, 2011, **56**(28), 10694–10700, DOI: 10.1016/j.electacta.2011.03.013.

45 G. J. Edens, X. Gao and M. J. Weaver, The Adsorption of Sulfate on Gold(111) in Acidic Aqueous Media: Adlayer Structural Inferences from Infrared Spectroscopy and Scanning Tunneling Microscopy, *J. Electroanal. Chem.*, 1994, 351–366.

46 K. Sato, S. Yoshimoto, J. Inukai and K. Itaya, Effect of Sulfuric Acid Concentration on the Structure of Sulfate Adlayer on Au(1 1 1) Electrode, *Electrochem. Commun.*, 2006, **8**(5), 725–730, DOI: 10.1016/j.elecom.2006.03.001.

47 A. I. Karelin and V. A. Tarasenko, The Water Activity and Free Water Mole Fraction in Perchloric Acid, *J. Solut. Chem.*, 2015, **44**(1), 146–151, DOI: 10.1007/s10953-014-0285-x.

48 L. Zhang, P. M. Grace and D.-W. Sun, An Accurate Water Activity Model for Sulfuric Acid Solutions and Its Implementation on Moisture Sorption Isotherm Determination, *Dry. Technol.*, 2022, **40**(12), 2540–2549, DOI: 10.1080/07373937.2020.1869037.

49 Y. Zhao, X. Hu, G. D. Stucky and S. W. Boettcher, Thermodynamic, Kinetic, and Transport Contributions to Hydrogen Evolution Activity and Electrolyte-Stability Windows for Water-in-Salt Electrolytes, *J. Am. Chem. Soc.*, 2024, **146**(5), 3438–3448, DOI: 10.1021/jacs.3c12980.

50 L. Suo, O. Borodin, T. Gao, M. Olguin, J. Ho, X. Fan, C. Luo, C. Wang and K. Xu, "Water-in-Salt" Electrolyte Enables High-Voltage Aqueous Lithium-Ion Chemistries, *Science*, 2015, **350**(6263), 938–943, DOI: 10.1126/science.aab1595.